Probing chirality fluctuations in molecules by nonlinear optical spectroscopy

N. Mann,[1,2] P. Nalbach,[1,2] S. Mukamel,[3] and M. Thorwart[1,2]
[1]*I. Institut für Theoretische Physik, Universität Hamburg, Jungiusstraße 9, 20355 Hamburg, Germany*
[2]*The Hamburg Centre for Ultrafast Imaging, Luruper Chaussee 149, 22761 Hamburg, Germany*
[3]*Department of Chemistry, University of California, Irvine, California 92697-2025, USA*

(Received 16 September 2014; accepted 28 November 2014; published online 16 December 2014)

Symmetry breaking caused by geometric fluctuations can enable processes that are otherwise forbidden. An example is a perylene bisimide dyad whose dipole moments are perpendicular to each other. Förster-type energy transfer is thus forbidden at the equilibrium geometry since the dipolar coupling vanishes. Yet, fluctuations of the geometric arrangement have been shown to induce finite energy transfer that depends on the dipole variance, rather than the mean. We demonstrate an analogous effect associated with chirality symmetry breaking. In its equilibrium geometry, this dimer is nonchiral. The linear chiral response which depends on the average geometry thus vanishes. However, we show that certain 2D chiral optical signals are finite due to geometric fluctuations. Furthermore, the correlation time of these fluctuations can be experimentally revealed by the waiting time dependence of the 2D signal. © *2014 AIP Publishing LLC*. [http://dx.doi.org/10.1063/1.4903858]

I. INTRODUCTION

Almost all biological molecules such as nuclear bases, sugars, and peptides are chiral. These chiral structures occur in enantiomer pairs connected by a reflection symmetry. While chiral enantiomers show large differences in their biological activity and their chemical reactivity, most physical properties are identical. Thus, only few physical methods are usable to study chirality.[1,2] Most commonly, the circular dichroism (CD),[3] the difference between the absorption of left- and right-handed circularly polarized light, is used. Equivalent information to that from CD can be obtained from the $I_{yz} - I_{zy}$ tensor component of the free induction decay signal for linearly polarized light propagating along the x-direction.[4] Often, chiral molecules have more than a single conformation which are thermally accessible at finite temperatures. Each conformation has its own chiral response, and, thus, only a thermal average over these conformations can be measured in the experiment.[5] Recently, nonlinear optical signals have been proposed as a measure for chirality. They, in addition, allow us to determine the relevant time scale of the chirality switching between conformations and enantiomers.[6] By these nonlinear optical signals, molecules can also be studied which are achiral in their equilibrium configuration, but show a finite chirality when thermal fluctuations of their configuration break spatial symmetry.[6] They can also reveal the correlation time of such thermal fluctuations directly in experiments. The nonlinear optical signals also provide useful information when they are obtained from molecules in the bulk after averaging over all molecular orientations. They in particular do not suffer from the artifacts of the fluorescence detected linear CD which even may occur in the linear dichroism in single immobilized molecules.[7]

Here, we focus on geometry fluctuations in a perylene bisimide donor acceptor (PBDA) pair. These have been shown to induce rather strong Förster resonant energy transfer (FRET) that is forbidden in the average geometry.[8] We extend the same idea to chirality and show that a molecule which is achiral in its equilibrium configuration may show signatures of chirality induced by geometry fluctuations in its nonlinear optical 2D spectrum.

FRET[9] is a well established and widely used measuring tool to determine the molecular proximity of light-absorbing and fluorescent structures.[10,11] These applications rely on the basic property of FRET that the energy transfer time is proportional to the dipolar coupling strength between the transition dipole moments $\vec{\mu}_j$ of the energy donor/acceptor ($j = 1/2$) spaced at distance R with connecting unit vector $\vec{\mathbf{n}}$, i.e., $\tau_{FRET} \propto ([\vec{\mu}_1\vec{\mu}_2 - 3(\vec{\mu}_1\vec{\mathbf{n}})(\vec{\mu}_2\vec{\mathbf{n}})]/R^3)^{-2}$. Accordingly, FRET vanishes for orthogonally arranged dipoles when $\vec{\mu}_1\vec{\mu}_2 = 0$ and $\vec{\mu}_i\vec{\mathbf{n}} = 0$. In this work, we consider a perylene bisimide donor acceptor pair, which is a heterodimer and has such a property. It has also been analyzed in recent experiments[12,13] and its chemical structure is sketched in Fig. 1. Surprisingly, despite the orthogonal arrangement, a fast energy transfer was measured with a transfer time of 9.4 ps for PBDA in chloroform.[13] It could be explained on the basis of angular thermal fluctuations in the geometric structure.[8] These angle fluctuations induce fluctuations of the dipolar energies and contribute to the FRET.[14,15] Treating the angle fluctuations as environmental fluctuations results in strong effective excitonic dipolar donor-acceptor couplings and thus in a considerable noise-induced energy transfer. The angular fluctuation strength can be estimated from the energy fluctuations which are observable by the optical Stokes' shifts. Then, the energy transfer time and its temperature dependence even quantitatively could be accounted for.[8] Moreover, the distance dependence of τ_{FRET} is modified to $\propto R^3$ as compared to $\propto R^6$ from standard Förster theory.[8]

The quantitative success of these results crucially depends on the relation between energy and angular fluctuations. The angular fluctuations are not directly accessible

experimentally so far which finally prevents an experimental verification. In equilibrium, the PBDA pair is an achiral molecular structure. However, angular fluctuations clearly break this symmetry and also result in a finite chirality. This can be quantified by the nonlinear spectroscopic signals, as it was proposed by Sanda and Mukamel.[6] We apply this concept of chirality fluctuations to the particular case of the PBDA pair and determine the chiral signals by treating the slow angular fluctuations as an Ornstein-Uhlenbeck process. We calculate for a finite fixed angle the $I_{yz} - I_{zy}$ tensor component of free induction decay for linearly polarized light propagating along the x-direction. This yields the information which is equivalent to the circular dichroism. We also study how the response changes when tuning the PBDA pair towards a homodimer. Such an arrangement in particular facilitates the investigation of the noise-induced energy transfer.[8] Then, we study the angle-averaged 2D chiral spectrum and its dependence on the waiting time. In particular, this allows us to determine the angle fluctuation correlation time and strength. We show quantitatively that the chirality fluctuations can be used to test the orthogonality of the dipoles in the PBDA pair on an entirely independent footing.

II. MODEL

A. Geometric setup

The focus of our study is an orthogonally arranged PBDA pair which is sketched in Fig. 1. To model excitonic energy transfer, the arrangement of the electric dipoles is relevant. Fig. 2 displays the perpendicular dipole moments $\boldsymbol{\mu}_1$ and $\boldsymbol{\mu}_2$ and the connecting vector $\mathbf{R}$, which is parallel to $\boldsymbol{\mu}_2$ and perpendicular to $\boldsymbol{\mu}_1$. Thus, $\mathbf{n} \perp \boldsymbol{\mu}_1 \perp \boldsymbol{\mu}_2$ and $\mathbf{n} \parallel \boldsymbol{\mu}_2$ and the dipole-dipole coupling strength

$$J = \frac{\boldsymbol{\mu}_1\boldsymbol{\mu}_2 - 3(\boldsymbol{\mu}_1\mathbf{n})(\boldsymbol{\mu}_2\mathbf{n})}{|\mathbf{R}|^3} \tag{1}$$

vanishes accordingly. Here, $\mathbf{n}$ is the unit vector in the direction of $\mathbf{R}$.

Since the donor and the acceptor are rigid, any deviation from the orthogonal arrangement of the dipoles should arise from rotations at the location of the chemical bonds between the spacer and the donor and between the spacer and the acceptor. In order to simplify the following calculations, we assume that the connecting vector fixes the coordinate system

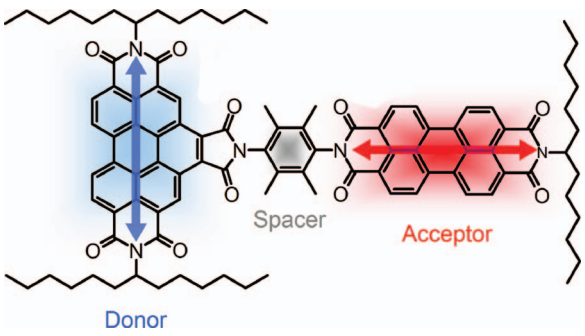

FIG. 1. Sketch of the chemical structure of an orthogonally arranged perylene bisimide donor acceptor pair (PBDA) together with the transition dipole moments.[12]

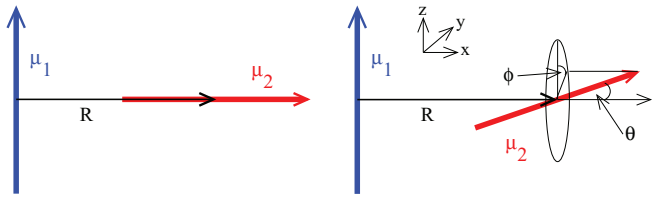

FIG. 2. Left: Sketch of the arrangement of the two transition dipole moments $\boldsymbol{\mu}_1$ and $\boldsymbol{\mu}_2$ and the connecting vector $\mathbf{R}$ of the PBDA pair. Right: Illustration of the angle θ and ϕ when $\boldsymbol{\mu}_2$ does not point along the x-axis.

and the two dipole moments can only rotate around their centers. Rotations of $\boldsymbol{\mu}_1$ might then result in a finite dipole-dipole coupling, but the PBDA is still achiral. In other words, since $\mathbf{n} \parallel \boldsymbol{\mu}_2$ any additional vector will span a plane with the former two vectors and the whole system is planar. Thus, a chiral signal can only result when $\boldsymbol{\mu}_2$ rotates out of the plane of $\boldsymbol{\mu}_1$ and $\mathbf{n}$, thereby forming a helical structure. For simplicity, we disregard rotations of $\boldsymbol{\mu}_1$ completely since for not too strong angular fluctuations, they will leave our results qualitatively unchanged.

To describe the rotation of $\boldsymbol{\mu}_2$, we introduce two angles. First, θ measures the angle between $\boldsymbol{\mu}_2$ and the x-axis. Second, ϕ denotes the angle between the projection of $\boldsymbol{\mu}_2$ in the $y-z$ plane and the z-axis (see Fig. 2). We note that rotations with $\phi = 0$ cause a finite dipolar coupling although the complex remains planar and thus achiral. For $\phi = \pi/2$, however, the complex is chiral but the dipolar coupling vanishes. To observe an optical chiral signal from and a finite energy transfer in the complex, both a finite dipolar coupling and a chiral geometry are necessary. Thus, we have to consider variations in both angles, θ and ϕ, in contrast to the somewhat simpler situation of the complex studied in Ref. 6.

Using the coordinate system defined in Fig. 2 (right panel), the dipole moments are parametrized according to

$$\begin{aligned} \boldsymbol{\mu}_1 &= (\mu_1)\hat{e}_z, \\ \boldsymbol{\mu}_2 &= (\mu_2 \cos\theta)\hat{e}_x + (\mu_2 \sin\theta \sin\phi)\hat{e}_y + (\mu_2 \sin\theta \cos\phi)\hat{e}_z. \end{aligned} \tag{2}$$

The dipolar coupling is

$$J \equiv J(\phi) = \frac{\mu_1\mu_2}{R^3} \sin\theta \cos\phi \tag{3}$$

with $R = |\mathbf{R}|$ and $\mathbf{R} = (R)\hat{e}_x$ and $J_0 = \mu_1\mu_2/R^3 \simeq 85\ \mathrm{cm}^{-1}$ for the PBDA pair.

B. Slow dynamics of angular movement

When the dipole moments fluctuate around their orthogonal arrangement, the angles evolve stochastically in time and induce a diffusive dynamics in a potential. In the simplest model, the potential is harmonic, and, in more detail, we expect a harmonic potential for the angle θ with equilibrium angle $\theta_0 = 0$ and free rotation about ϕ. For a stochastic time evolution of θ, we assume slow movements described by an Ornstein-Uhlenbeck process. This results in an equilibrium density for θ of the form

$$\rho_\theta^{\mathrm{eq}}(\theta) = \frac{1}{\sigma\sqrt{2\pi}} \exp\left[-\frac{\theta^2}{2\sigma^2}\right] \tag{4}$$

and a probability density to observe θ at time t when the original angle at initial time 0 was θ' as

$$\mathcal{P}_\theta(\theta,\theta',t) = \frac{1}{2\sigma^2\pi\sqrt{1-e^{-2Dt}}} \times \exp\left[-\frac{\theta^2+\theta'^2-2\theta\theta' e^{-Dt}}{2\sigma^2(1-e^{-2Dt})}\right]. \quad (5)$$

Herein, the diffusion constant D is the inverse autocorrelation time of the fluctuations. Comparing this description with a system-bath approach (as employed in Ref. 8), $D^{-1} = \omega_c \lesssim 2500\ \mathrm{cm}^{-1}$. Here, ω_c is the high-energy cutoff of the environmental spectral density. The dependence of the chiral 2D spectra on the waiting time determined below will allow us to extract D from experimental data. The width of the angular distribution is $\sigma^2 = \langle\theta^2\rangle$. In Ref. 8, the angular reorganization energy was estimated as $\lambda_\theta \simeq 1\ \mathrm{cm}^{-1}$. At high temperatures, we have that $\lambda_\theta = \frac{1}{2}\langle J_0^2\theta^2\rangle/(k_\mathrm{B}T)$ with $J_0 = \mu_1\mu_2/R^3 \simeq 85\ \mathrm{cm}^{-1}$. Thus, we may estimate at room temperature for the PBDA pair under consideration the width of $\sigma \simeq 0.24$.

For the angle ϕ, we assume a homogeneous equilibrium probability density $\rho_\phi^{\mathrm{eq}}(\phi) = 1/(2\pi)$. It is reasonable to expect for the dynamics of ϕ a similar form as for the θ-dynamics, but the corresponding width is $\sigma_\phi \to \infty$, since free rotation is possible. Since we are interested on the time scales of the diffusive angular dynamics and shorter, we also model the dynamics for computational simplicity by the form

$$\mathcal{P}_\phi(\phi,\phi',t) = \frac{1}{2\sigma_\phi^2\pi\sqrt{1-e^{-2Dt}}} \times \exp\left[-\frac{\phi^2+\phi'^2-2\phi\phi' e^{-Dt}}{2\sigma_\phi^2(1-e^{-2Dt})}\right] \quad (6)$$

with $\sigma_\phi = 2\pi$.

C. Hamiltonian

The PBDA pair is a heterodimer. Describing each monomer as a quantum two-level system, the dimer is described by a Frenkel exciton Hamiltonian

$$H = \frac{1}{2}\epsilon_1\sigma_z^{(1)} + \frac{1}{2}\epsilon_2\sigma_z^{(2)} + J\sigma_x^{(1)}\sigma_x^{(2)}, \quad (7)$$

with the standard Pauli matrices $\sigma_{x,z}^{(j=1,2)}$. It is readily diagonalized by the transformation

$$\hat{T} = \exp\left(\frac{i}{2}\alpha\sigma_y^{(1)}\sigma_x^{(2)} + \frac{i}{2}\beta\sigma_x^{(1)}\sigma_y^{(2)}\right) \quad (8)$$

with the angles α and β following from

$$\tan(\alpha+\beta) = -\frac{J}{\epsilon} \quad \text{and} \quad \tan(\alpha-\beta) = -\frac{J}{\delta\epsilon}$$

with $\epsilon = \frac{1}{2}(\epsilon_1+\epsilon_2)$ and $\delta\epsilon = \frac{1}{2}(\epsilon_1-\epsilon_2)$. For the PBDA heterodimer under consideration, $\delta\epsilon \simeq 2500\ \mathrm{cm}^{-1}$. This leads to two independent effective two-level systems described by the Pauli matrices $\tau_z^{(j=+,-)}$ with the Hamiltonian

$$H_d = \hat{T}H\hat{T}^\dagger = \frac{1}{2}E_+\tau_z^{(+)} + \frac{1}{2}E_-\tau_z^{(-)} \quad (9)$$

with $E_\pm = \sqrt{J^2+\epsilon^2} \pm \sqrt{J^2+\delta\epsilon^2}$.

D. Light-matter interaction

The total dipole moment $\hat{\boldsymbol{\mu}} = \boldsymbol{\mu}_1\sigma_x^{(1)} + \boldsymbol{\mu}_2\sigma_x^{(2)}$ of the dimer is transformed in the same way leading to

$$\hat{\boldsymbol{\mu}} = \boldsymbol{\mu}_1\left[\gamma_1\tau_x^{(+)} - \gamma_3\tau_z^{(+)}\tau_x^{(-)}\right] + \boldsymbol{\mu}_2\left[\gamma_4\tau_x^{(-)} - \gamma_2\tau_x^{(+)}\tau_z^{(-)}\right]$$

with $\gamma_1 = \cos\alpha$, $\gamma_2 = \sin\beta$, $\gamma_3 = \sin\alpha$, and $\gamma_4 = \cos\beta$.

The two effective two-level systems can be spectroscopically addressed independently, and thus we focus on the response of the $\tau_\pm$ systems. The corresponding dipole components are

$$\hat{\boldsymbol{\mu}}_+ = \left[\boldsymbol{\mu}_1\gamma_1 - \boldsymbol{\mu}_2\gamma_2\tau_z^{(-)}\right]\tau_x^{(+)},$$
$$\hat{\boldsymbol{\mu}}_- = \left[-\boldsymbol{\mu}_1\gamma_3\tau_z^{(+)} + \boldsymbol{\mu}_2\gamma_4\right]\tau_x^{(-)}.$$

Since $\epsilon \gg \delta\epsilon \gtrsim J \simeq k_\mathrm{B}T$, we have that $\alpha \simeq -\beta$ and thus $\tan(2\alpha) = -J/\delta\epsilon$. At the same time, $\gamma_1 = \gamma_4$ and $\gamma_3 = -\gamma_2$. Typically, optical spectroscopic experiments start with the system in the ground state. Hence, we may simplify

$$\begin{aligned}\hat{\boldsymbol{\mu}}_+ &\simeq [\gamma_1\boldsymbol{\mu}_1 + \gamma_2\boldsymbol{\mu}_2]\tau_x^{(+)} \\ &= [(\gamma_2\mu_2\cos\theta)\hat{e}_x + (\gamma_2\mu_2\sin\theta\sin\phi)\hat{e}_y \\ &\quad + (\gamma_1\mu_1 + \gamma_2\mu_2\sin\theta\cos\phi)\hat{e}_z], \end{aligned} \quad (10)$$

and similarly,

$$\begin{aligned}\hat{\boldsymbol{\mu}}_- &\simeq [-(\gamma_1\mu_2\cos\theta)\hat{e}_x - (\gamma_1\mu_2\sin\theta\sin\phi)\hat{e}_y \\ &\quad + (\gamma_2\mu_1 - \gamma_1\mu_2\sin\theta\cos\phi)\hat{e}_z]. \end{aligned} \quad (11)$$

In the following, we use the notation $\gamma_1 \equiv \gamma_1(\phi) = J(\phi)/\mathcal{N}(\phi)$ and $\gamma_2 \equiv \gamma_2(\phi) = (\sqrt{\delta\epsilon^2+J^2(\phi)} - \delta\epsilon)/\mathcal{N}(\phi)$ with $\mathcal{N}^2 = J^2 + (\delta\epsilon - \sqrt{\delta\epsilon^2+J^2})^2$.

Standard multipole expansion of the interaction with the laser electric field generates effective magnetic dipoles and electric quadrupoles.[6] Those typically dominate over the contributions from real magnetic dipoles and electric quadrupoles of the two monomers.[16] In the following, we neglect the latter. Then, we combine the effective magnetic dipole moment $\mathbf{M}_\pm$ and the effective electric quadrupole tensor $\mathbf{Q}_\pm$ to obtain the tensor

$$T_{\pm,\alpha\beta} = -iR_\alpha\mu_{\mp,\beta}/2 = iQ_{\pm,\alpha\beta} - \varepsilon_{\alpha\beta\gamma}M_{\pm,\gamma}/k, \quad (12)$$

with $R_{\alpha=x,y,z}$ being the components of the distance vector $\mathbf{R}$. k is the absolute value of the wave vector of the incident laser field and where $Q_{\pm,\alpha\beta}$ is symmetric and $\varepsilon_{\alpha\beta\gamma}M_{\pm,\gamma}$ antisymmetric. We find

$$T_- = -\frac{iR}{2}\begin{pmatrix} \gamma_2\mu_2\cos\theta & 0 & 0 \\ \gamma_2\mu_2\sin\theta\sin\phi & 0 & 0 \\ \gamma_1\mu_1 + \gamma_2\mu_2\sin\theta\cos\phi & 0 & 0 \end{pmatrix}, \quad (13)$$

$$T_+ = -\frac{iR}{2}\begin{pmatrix} -\gamma_1\mu_2\cos\theta & 0 & 0 \\ -\gamma_1\mu_2\sin\theta\sin\phi & 0 & 0 \\ \gamma_2\mu_1 - \gamma_1\mu_2\sin\theta\cos\phi & 0 & 0 \end{pmatrix}, \quad (14)$$

and

$$Q_- = -\frac{R}{4}\cdot\begin{pmatrix} 2\gamma_2\mu_2\cos\theta & \gamma_2\mu_2\sin\theta\sin\phi & \gamma_1\mu_1+\gamma_2\mu_2\sin\theta\cos\phi \\ \gamma_2\mu_2\sin\theta\sin\phi & 0 & 0 \\ \gamma_1\mu_1+\gamma_2\mu_2\sin\theta\cos\phi & 0 & 0 \end{pmatrix},$$

$$Q_+ = -\frac{R}{4}\cdot\begin{pmatrix} -2\gamma_1\mu_2\cos\theta & -\gamma_1\mu_2\sin\theta\sin\phi & \gamma_2\mu_1-\gamma_1\mu_2\sin\theta\cos\phi \\ -\gamma_1\mu_2\sin\theta\sin\phi & 0 & 0 \\ \gamma_2\mu_1-\gamma_1\mu_2\sin\theta\cos\phi & 0 & 0 \end{pmatrix}.$$

Moreover, the electric dipole moments assume the form

$$\mathbf{M}_- = -\frac{ikR}{4}(0,\ \gamma_1\mu_1+\gamma_2\mu_2\sin\theta\cos\phi,\ -\gamma_2\mu_2\sin\theta\sin\phi)^T,$$
$$\mathbf{M}_+ = -\frac{ikR}{4}(0,\ \gamma_2\mu_1-\gamma_1\mu_2\sin\theta\cos\phi,\ \gamma_1\mu_2\sin\theta\sin\phi)^T.$$

The interaction Hamiltonian of a laser pulse with field $\mathbf{F}(t)\exp(i\mathbf{k}\mathbf{R}/2)$ with the dimer in the rotating wave approximation[17] and to first order in $k = |\mathbf{k}|$ only reads

$$H_{\rm int} = -\sum_{\alpha=x,y,z}\sum_{j=\pm} F_\alpha \tau_\uparrow^{(j)}\Big\{\mu_{j,\alpha} + i\sum_{\beta=x,y,z} k_\beta Q_{j,\alpha\beta} - \sum_{\beta,\gamma=x,y,z}\varepsilon_{\alpha\beta\gamma}k_\beta M_{j,\gamma}\Big\} + \text{h.c.} \quad (15)$$

with $\tau_\uparrow^{(j)} = \frac{1}{2}(\tau_x^{(j)} + i\tau_y^{(j)})$. Moreover, F_α are the field components of $\mathbf{F}$.

III. CHIRAL LINEAR RESPONSE

We assume that the two frequencies $E_\pm$ can be probed separately and focus in the following on E_+ which results in a simplified effective field-matter interaction Hamiltonian $H_{\rm int} = -F_\alpha(t)\mathcal{J}_\alpha\tau_\uparrow + \text{h.c.}$ with $\mathcal{J}_\alpha = \mu_\alpha + k_\beta T_{\alpha\beta} + \mathcal{O}(k^2)$. The tensor elements $T_{\alpha\beta}$ follow from Eq. (12) after omitting the index (+). Moreover, repeated Greek symbols are summed over.

Linear optical response is given by the correlation function $I_{\alpha\beta}(t) = \langle\mathcal{J}_\alpha(t)\mathcal{J}_\beta(0)\rangle$. Experimentally, the response of single molecules is rarely accessible. Instead ensembles are investigated with each molecule with arbitrary orientation in space. Thus, orientational averaging (denoted by $\langle\cdot\rangle_\Omega$ in the following) over the solid angle Ω is performed following standard rules.[18] This finally results in

$$I_{\alpha\beta}(t) = \frac{1}{3}\delta_{\alpha\beta}\langle\mu_\gamma^*(t)\mu_\gamma(0)\rangle_\Omega + \frac{1}{3}\varepsilon_{\alpha\beta\gamma}k_\gamma[\langle M_\delta^*(t)\mu_\delta(0)\rangle_\Omega - \langle\mu_\delta^*(t)M_\delta(0)\rangle_\Omega]. \quad (16)$$

Only the second part is a chiral signal. With light propagating along the x-direction, i.e., $k_\alpha = k\delta_{\alpha,x}$, we can observe the chiral component by measuring

$$I_{yz}^\pm(t) \approx \frac{2i}{3}\int d\theta\rho_\theta^{eq}(\theta)\int\frac{d\phi}{2\pi}\cdot\text{Im}\{M_\delta^*(\theta,\phi)\mu_\delta(\theta,\phi)\}e^{-\Gamma t}e^{-iE_\pm(\theta,\phi)t}. \quad (17)$$

Here, we have assumed that the angles vary only slowly on internal system time scales such that we may set $\phi(t) \approx \phi(0)$ and $\theta(t) \approx \theta(0)$. Herein, Γ is the dephasing rate. We assume throughout the paper a dephasing time of ∼100 fs corresponding to $\Gamma = 50\ \text{cm}^{-1}$. Fourier transforming the integrand results in

$$\mathcal{I}_{yz}^\pm(\omega,\theta,\phi) = \pm\frac{kR\mu_1\mu_2}{6(2\pi)}\cdot\sin\theta\sin\phi\cdot\rho_\theta^{\rm eq}(\theta)\times\frac{\omega - E_\pm(\theta,\phi) - i\Gamma}{[\omega - E_\pm(\theta,\phi)]^2+\Gamma^2}. \quad (18)$$

This function is antisymmetric in ϕ and θ. Thus, on average the chiral linear response vanishes. Note that each angle average separately results already in a vanishing chiral signal.

Fig. 3 shows the real (upper row) and the imaginary (lower row) part of the chiral linear signal color coded versus frequency ω and angle ϕ with fixed $\theta = \pi/4$. We use the parameters as extracted in Ref. 8, i.e., $J = 85\ \text{cm}^{-1}$, $\Gamma = 50\ \text{cm}^{-1}$, and the standard deviation $\sigma = 0.24$ for the θ-angle fluctuations. We show the results for three different values of $\delta\epsilon$, i.e., $\delta\epsilon = 2500\ \text{cm}^{-1}$ (left column), which corresponds to the PBDA pair experimentally studied,[8] then $\delta\epsilon = 85\ \text{cm}^{-1}$ (middle column) and $25\ \text{cm}^{-1}$ (right column). For $\phi = 0$, the complex is achiral and no signal is observed. For finite ϕ, we observe a double peak structure with opposite sign for the real part and a single peak in the imaginary part for varying frequency. For a fixed ω, we also observe a double peak structure when ϕ is varied for $\delta\epsilon = 2500\ \text{cm}^{-1}$ (left column). With decreasing $\delta\epsilon$, however, the peak form (of the imaginary part and of the peak at lower frequency in the real part) changes towards a *heart* shape exhibiting (for some ω) two positive peaks followed by two negative ones. We note that the case of small $\delta\epsilon$ is closer to a homodimer. Similar results are expected, when the structure would fluctuate around a chiral equilibrium with $\phi \neq 0$ and $\theta \neq 0$. Those could be used to determine the geometric structure of such complexes.

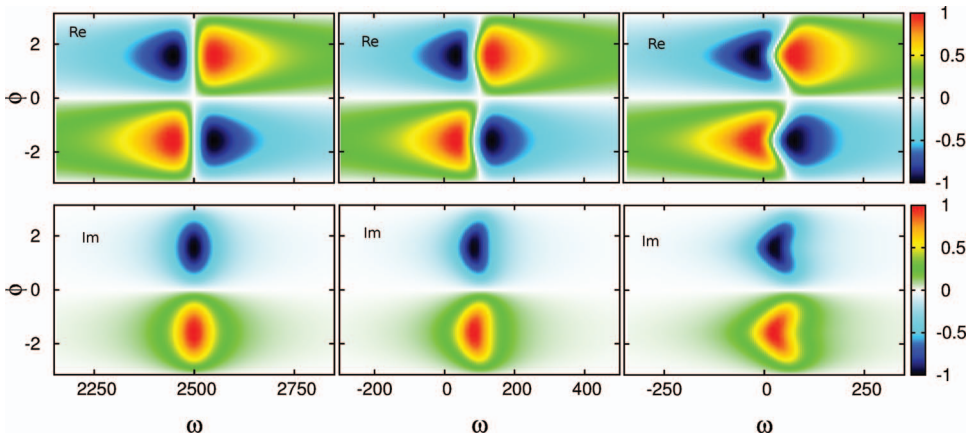

FIG. 3. Real (upper row) and the imaginary (lower row) part of the chiral linear spectrum versus frequency ω and angle ϕ with fixed $\theta = \pi/4$ for $J = 85\ \mathrm{cm}^{-1}$, $\Gamma = 50\ \mathrm{cm}^{-1}$, $\sigma = 0.24$ and $\delta\epsilon = 2500\ \mathrm{cm}^{-1}$ (left column), $\delta\epsilon = 85\ \mathrm{cm}^{-1}$ (middle column), and $25\ \mathrm{cm}^{-1}$ (right column).

IV. 2D CHIRAL SPECTRUM

Next, we focus on nonlinear chiral signals, in particular on 2D chiral spectra. We determine the 4-point correlation function[6]

$$\mathcal{R}_c = \mathcal{R}^{xx}_{[yz][yz]} + 2\mathcal{R}^{zx}_{[xy][yz]}, \tag{19}$$

which yields a purely chiral 2D signal. Therein, $\mathcal{R}^{zx}$ represents the response in a setup where the first two pulses propagate along the x-direction and the third pulse and the detection is along the z-direction. Correspondingly, $\mathcal{R}^{xx}$ represents a collinear arrangement with all pulses and detection along the x-direction. The subscripts are short-hand notations for

$$\mathcal{R}^{zx}_{[xy][yz]} = \mathcal{R}^{zx}_{xyyz} - \mathcal{R}^{zx}_{yxyz} - \mathcal{R}^{zx}_{xyzy} + \mathcal{R}^{zx}_{yxzy},$$
$$\mathcal{R}^{xx}_{[yz][yz]} = \mathcal{R}^{xx}_{yzyz} - \mathcal{R}^{xx}_{zyyz} - \mathcal{R}^{xx}_{yzzy} + \mathcal{R}^{xx}_{zyzy},$$

and

$$\mathcal{R}_{\alpha\beta\gamma\delta} = \langle \mathcal{J}^*_\alpha(\tau_3)\mathcal{J}_\beta(\tau_2)\mathcal{J}_\gamma(\tau_1)\mathcal{J}^*_\delta(0)\rangle_\Omega, \tag{20}$$

with $\mathcal{J}_\alpha = \mu_\alpha + k_\beta T_{\alpha\beta} + \mathcal{O}(k^2)$ as defined before. Thus, the subscripts in $\mathcal{R}_{\alpha\beta\gamma\delta}$ denote the polarization of the pulses, i.e., α for the first pulse, β and γ for the second and third one, and δ for the detection. In the following, we focus on the τ^+-subsystem. Thereby, we neglect coherences between the τ^+ and τ^- subsystems on the basis of assuming the laser pulses to be spectrally narrower than the energy difference $E_+ - E_-$. For this situation, cross peaks were shown to yield no clear chiral signatures.[6] Hence, we may concentrate on the diagonal peaks.

Optical signals associated to a chirality exchange result from the two-time correlation of the pseudo-scalar $\boldsymbol{\mu}\cdot\mathbf{M}$. These are weak signals and they scale as $\propto(kR)^2$.

We next determine their contribution to the 4-point correlation function $\mathcal{R}_c$. All contributions which are linear in kR vanish after the orientational averaging (see Appendix D in Ref. 6). Likewise, the zeroth order contributions coming from $\mathcal{R}^{zx}_{[xy][yz]}$ also vanish for the same reason. Yet, we may consider

$$\mathcal{R}^{xx}_{[yz][yz]} \propto [\langle \mathcal{J}^*_\alpha(\tau_3)\mathcal{J}_\beta(\tau_2)\mathcal{J}_\alpha(\tau_1)\mathcal{J}^*_\beta(0)\rangle_\Omega - \langle \mathcal{J}^*_\alpha(\tau_3)\mathcal{J}_\beta(\tau_2)\mathcal{J}_\beta(\tau_1)\mathcal{J}^*_\alpha(0)\rangle_\Omega].$$

In case of very fast angular fluctuations, we could average over ϕ and θ separately at all times τ_i resulting in a vanishing $\mathcal{R}^{xx}_{[yz][yz]}$. Typically, however, angular motion is slow compared to the internal system time scales. Thus, a significant signal strength is only observed at experimental times $t_1 = \tau_1$ and $t_3 = \tau_3 - \tau_2$, over which the 2D Fourier transform is later performed, for which $Dt_1, Dt_3 \ll 1$ holds. Thus, the angles do not change during these time intervals. However, the waiting time $t_2 = \tau_2 - \tau_1$ is experimentally varied over much longer times and accordingly angular motion during this time interval has to be taken into account. This is done by employing the above introduced probability densities to observe θ and ϕ at time t_2 when originally at time 0 the angles were θ' and ϕ'. Thus, we calculate in detail

$$\begin{aligned}&\langle \mathcal{J}^*_\alpha(\tau_3)\mathcal{J}_\beta(\tau_2)\mathcal{J}_\gamma(\tau_1)\mathcal{J}^*_\delta(0)\rangle_\Omega \\ &= \int d\theta \int d\theta' \int d\phi \int d\phi' \\ &\quad\times \mathcal{P}_\phi(\phi,\phi',t_2)\mathcal{P}_\theta(\theta,\theta',t_2) \\ &\quad\times \langle \mathcal{J}^*_\alpha(\tau_3,\theta,\phi)\mathcal{J}_\beta(\tau_2,\theta,\phi)\mathcal{J}_\gamma(\tau_1,\theta',\phi')\mathcal{J}^*_\delta(0,\theta',\phi')\rangle_\Omega.\end{aligned} \tag{21}$$

Thus, for slow angular fluctuations, $\mathcal{R}^{xx}_{[yz][yz]}$ yields no zeroth order contribution.[19] Thus, all zeroth and first order contributions, i.e., $\propto(kR)^0$ and $\propto(kR)^1$, vanish and $\mathcal{R}_c(t_3,t_2,t_1) \propto (kR)^2$. Possible contributions to that order from contributions due to the light-matter interaction also vanish due to the same arguments[6] (note that we have neglected these terms above already).

Thus, $\mathcal{R}_c$ is dominated by contributions from the two-time correlations of the pseudo-scalar $\boldsymbol{\mu}\cdot\mathbf{M}$ of order $\propto(kR)^2$. Following the derivation of Sanda and Mukamel,[6] we find that

$$\mathcal{R}_c(t_3,t_2,t_1) = -\frac{2k^2}{3}[\langle X_{\alpha\beta\gamma\gamma\beta\alpha}\rangle_\Omega + 2\langle X_{\alpha\beta\gamma\beta\alpha\gamma}\rangle_\Omega], \tag{22}$$

with the definition

$$\begin{aligned}X_{\alpha\beta\gamma\delta\xi\eta} = &[-\mathrm{Im}\{T_{\alpha\beta}(\tau_2)\mu^*_\gamma(\tau_2)\} + \mathrm{Im}\{T_{\gamma\beta}(\tau_2)\mu^*_\alpha(\tau_2)\}] \\ &\cdot[-\mathrm{Im}\{T_{\delta\xi}(0)\mu^*_\eta(0)\} + \mathrm{Im}\{T_{\eta\xi}(0)\mu^*_\delta(0)\}].\end{aligned}$$

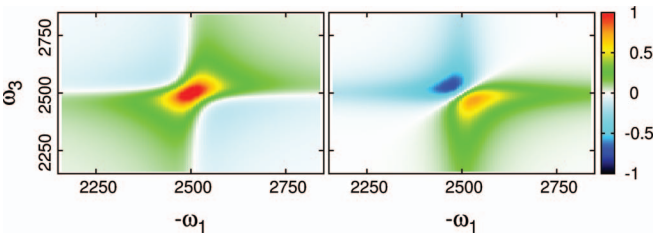

FIG. 4. Real (left) and imaginary part of $\mathcal{R}_c(\omega_3, t_2, \omega_1)$ for very short waiting times $Dt_2 = 10^{-5}$ for the PBDA pair with $J = 85\ \mathrm{cm}^{-1}$, $\delta\epsilon = 2500\ \mathrm{cm}^{-1}$, and $\sigma_\phi = 2\pi$ and $\sigma_\theta = 0.24$.

For our PBDA dimer, we have that

$$\langle X_{\alpha\beta\gamma\gamma\beta\alpha}\rangle = -2\left(\frac{R}{2}\right)^2 \mu_1^2\mu_2^2 \cdot \langle \cos\theta_2 \cos\theta_0 + \sin\theta_2 \sin\phi_2 \sin\theta_0 \sin\phi_0\rangle_\Omega,$$

$$\langle X_{\alpha\beta\gamma\beta\alpha\gamma}\rangle = \left(\frac{R}{2}\right)^2 \mu_1^2\mu_2^2 \langle \cos\theta_2 \cos\theta_0\rangle_\Omega,$$

with $\theta_i \equiv \theta(\tau_i)$ and ϕ_i likewise.

Next, we observe that the energy $E_+ \equiv E_+(\theta, \phi)$ is a function of the angles θ and ϕ and that the primed energy means that the energy depends on the primed angles. With $t_1 = \tau_1$, $t_2 = \tau_2 - \tau_1$, and $t_3 = \tau_3 - \tau_2$, we obtain after a Fourier transformation with respect to the times t_1 and t_3 that

$$\mathcal{R}_c(\omega_3, t_2, \omega_1) = \frac{(kR)^2}{3}\mu_1^2\mu_2^2 \iiint d\theta d\theta' d\phi d\phi' \times \mathcal{P}_\phi(\phi, \phi', t_2)\mathcal{P}_\theta(\theta, \theta', t_2) r(\theta, \phi, \theta', \phi') \tag{23}$$

with

$$r(\theta, \phi, \theta', \phi') = \sin\theta \sin\phi \sin\theta' \sin\phi' \times \frac{\Gamma + i(\omega_3 - E_+)}{\Gamma^2 + (\omega_3 - E_+)^2} \frac{\Gamma + i(\omega_1 + E'_+)}{\Gamma^2 + (\omega_1 + E'_+)^2}. \tag{24}$$

Fig. 4 shows the 2D chiral signal $\mathcal{R}_c(\omega_3, t_2, \omega_1)$ for a very short waiting time $Dt_2 = 10^{-5}$. We employ the parameters of the PBDA pair, i.e., $J = 85\ \mathrm{cm}^{-1}$, $\delta\epsilon = 2500\ \mathrm{cm}^{-1}$, and $\sigma_\phi = 2\pi$ and $\sigma_\theta = 0.24$. The left (right) panel depicts the real (imaginary) part. Similar peak shapes are observed for smaller $\delta\epsilon$ and for longer waiting times. The peak shape reflects the assumption of a Markovian dephasing dynamics which is inherent to our assumption of the dephasing taken in the form of an exponential decay with a fixed dephasing time Γ. The integrand $r(\theta, \phi, \theta', \phi')$ determines which angular conformation dominantly contributes to the signal. As expected, these are the chiral conformations $\boldsymbol{\mu}_2 \perp \boldsymbol{\mu}_1 \parallel \mathbf{n} \perp \boldsymbol{\mu}_2$.

We expect that the overall strength of the nonlinear chiral signal rapidly decreases with increasing waiting times on a time scale determined by the autocorrelation time of the angular fluctuations. This is depicted in Fig. 5 which shows the maximal amplitude $R(t_2) = \max_{\omega_1,\omega_3} \mathcal{R}_c(\omega_3, t_2, \omega_1)$ scaled to $R_0 = R(t_2 = 10^{-5}D^{-1})$. Nonlinear chiral signals are in general weak since typically $(kR)^2 \sim 10^{-6}$. The fact that only non-vanishing fluctuations lead in the present case to a finite contribution to the signal only reduces the signal strength by another factor $R_0 \simeq 0.08$. In turn, by determining the peak maximum of the chiral 2D signal $\mathcal{R}_c(\omega_3, t_2, \omega_1)$ for various waiting times, one can experimentally measure the autocorrelation time of the angular fluctuations.

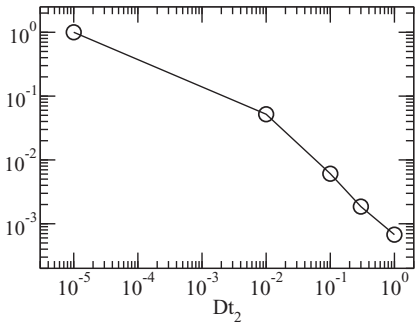

FIG. 5. Maximal amplitude of the real part $R(t_2) = \max_{\omega_1,\omega_3} \mathcal{R}_c(\omega_3, t_2, \omega_1)$ scaled to $R_0 = R(t_2 = 10^{-5}D^{-1})$ versus waiting times Dt_2 for $J = 85\ \mathrm{cm}^{-1}$, $\delta\epsilon = 2500\ \mathrm{cm}^{-1}$, and $\sigma_\phi = 2\pi$ and $\sigma_\theta = 0.24$.

V. CONCLUSIONS

We have determined the linear and 2D optical chiral spectra for a dimer system whose dipole moments are orthogonal with a connecting vector orthogonal to one of the dipoles. In its equilibrium configuration, the dimer is achiral and no chiral signal is expected. At the same time, the dipolar coupling vanishes and no Förster-type energy transfer arises. Geometrical fluctuations, however, result in finite dipolar couplings, causing rather fast energy transfer which has been experimentally observed. We show that to assign the fast energy transfer unambiguously to angular fluctuations around an orthogonal equilibrium configuration, chiral signals can be used. As long as the dimer configuration fluctuates around an orthogonal equilibrium configuration, the linear chiral spectrum vanishes, but is non-zero for (fluctuating) non-orthogonal configurations. The nonlinear 2D spectrum vanishes in the equilibrium configuration but is non-zero when angular fluctuations are present as long as the waiting time is short compared to the autocorrelation time of the fluctuations. This, in turn, can be used to determine the autocorrelation times experimentally. Hence, our approach may also be used to reveal correlation times of fluctuations which are otherwise hardly accessible experimentally.

ACKNOWLEDGMENTS

We acknowledge support by the Deutsche Forschungsgemeinschaft (DFG) Sonderforschungsbereich 925 "Light-induced dynamics and control of correlated quantum systems" (Project C8) and by the DFG excellence cluster "The Hamburg Center for Ultrafast Imaging." S.M. gratefully acknowledges the support of the National Science Foundation (NSF) through Grant No. CHE 1361516 , National Institutes of Health (NIH) Grant No. GM-59230, and the Chemical Sciences, Geosciences and Biosciences Division, Office of Basic

Energy Sciences, Office of Science, (U.S.) Department of Energy (DOE).

[1]P. Mukhopadhyay, P. Wipf, and D. N. Beratan, Acc. Chem. Res. **42**, 809 (2009).
[2]M. Quack, J. Stohner, and M. Willeke, Annu. Rev. Phys. Chem. **59**, 741 (2008).
[3]*Circular Dichroism: Principles and Applications*, edited by N. Berova, K. Nakanishi, and R. W. Woody (Wiley, New York, 2000).
[4]J. H. Choi, S. Cheon, H. Lee, and M. Cho, Phys. Chem. Chem. Phys. **10**, 3839 (2008).
[5]F. J. Devlin, P. J. Stephens, C. Österle, K. B. Wiberg, J. R. Cheeseman, and M. J. Frisch, J. Org. Chem. **67**, 8090 (2002).
[6]F. Sanda and S. Mukamel, J. Chem. Phys. **135**, 194201 (2011).
[7]Y. Tang, T. A. Cook, and A. E. Cohen, J. Phys. Chem. A **113**, 6213 (2009).
[8]P. Nalbach, I. Pugliesi, H. Langhals, and M. Thorwart, Phys. Rev. Lett. **108**, 218302 (2012).
[9]T. Förster, Ann. Phys. **437**, 55 (1948).
[10]V. May and O. Kühn, *Charge and Energy Transfer Dynamics in Molecular Systems*, 2nd ed. (Wiley-VCH, Weinheim, 2004).
[11]H. van Amerongen, L. Valkunas, and R. van Grondelle, *Photosynthetic Excitons* (World Scientific, Singapore, 2000).
[12]H. Langhals, S. Poxleitner, O. Krotz, T. Pust, and A. Walter, Eur. J. Org. Chem. **2008**, 4559 (2008).
[13]H. Langhals, A. J. Esterbauer, A. Walter, E. Riedle, and I. Pugliesi, J. Am. Chem. Soc. **132**, 16777 (2010).
[14]S. Jang, J. Chem. Phys. **127**, 174710 (2007).
[15]D. Beljonne, C. Curutchet, G. D. Scholes, and R. J. Silbey, J. Phys. Chem. B **113**, 6583 (2009).
[16]O. J. G. Somsen, R. van Grondelle, and H. van Amerogen, Biophys. J. **71**, 1934 (1996).
[17]B. Thimmel, P. Nalbach, and O. Terzidis, Eur. Phys. J. B **9**, 207 (1999).
[18]D. L. Andrews and T. Thirunamachandran, J. Chem. Phys. **67**, 5026 (1977).
[19]To treat the case where the angular motion happens on the same time scale as the internal system time scales $E_{\pm}^{-1}$, a full quantum mechanical treatment of the angular dynamics would be required.